 doi:10.20944/preprints202009.0398.v1

*Type of the Paper (Article)*

# Physicochemical and rheological properties of a transparent asphalt binder modified with nano-$TiO_2$

**Iran Rocha Segundo [1,*], Salmon Landi Jr. [2], Alexandros Margaritis [3], Georgios Pipintakos [3], Elisabete Freitas [1], Cedric Vuye [3], Johan Blom [3], Tom Tytgat [4], Siegfried Denys [4] and Joaquim Carneiro [5]**

[1] Department of Civil Engineering, University of Minho, Portugal,
[2] Federal Institute Goiano, Brazil,
[3] Energy and Materials in Infrastructure and Buildings (EMIB) Research Group, University of Antwerp, Belgium,
[4] Research Group Sustainable Energy, Air and Water Technology, University of Antwerp, Belgium,
[5] Centre of Physics, University of Minho, Portugal.
* Correspondence: iran_gomes@hotmail.com

**Abstract:** Transparent binder is used to substitute conventional black asphalt binder and to provide light-colored pavements, whereas nano-$TiO_2$ has the potential to promote photocatalytic and self-cleaning properties. Together, these materials provide multifunction effects and benefits when the pavement is submitted to high solar irradiation. This paper analyses the physicochemical and rheological properties of a transparent binder modified with 0.5%, 3.0%, 6.0%, and 10.0% of nano-$TiO_2$ and compares it to the transparent base binder, and conventional and polymer modified binders (PMB) without nano-$TiO_2$. Their penetration, softening point, dynamic viscosity, master curve, black diagram, Linear Amplitude Sweep (LAS), Multiple Stress Creep Recovery (MSCR), and Fourier-Transform Infrared Spectroscopy (FTIR) were obtained. The transparent binders (base and modified) seem to be workable considering their viscosity and exhibited values between the conventional binder and PMB regarding rutting resistance, penetration, and softening point. They showed similar behavior as the PMB, demonstrating signs of polymer-modification. The addition of $TiO_2$ seems to reduce fatigue life, except for the 0.5% content. Nevertheless, its addition in high contents increases the rutting resistance. The $TiO_2$ modification seems to have little effect on the chemical functional indices. The best percentage of $TiO_2$ was 0.5%, considering fatigue and 10.0% concerning permanent deformation.

**Keywords:** asphalt binder; transparent binder; nanomaterials; $TiO_2$; viscoelastic properties; FTIR; photocatalytic asphalt; light-colored asphalt; self-cleaning.

## 1. Introduction

Light and heat are essential influencing factors for asphalt pavements. Firstly, it is well known that they are essential keys for the asphalt binder aging, causing damages to the asphalt roads [1,2]. The absence of light profoundly affects the visibility condition, decreasing safety [3]. In contrast, a large amount of heating can increase the Urban Heat Island (UHI) effect in urban areas [4]. The conventional black color of asphalt pavements absorbs light and stores a large amount of thermal energy. Thus, for specific applications, it is important to control the light absorption and thermal energy storage in asphalt pavements, which can be carried out by the application of light-colored pavements [3].

Industrial activities and road traffic are the primary sources of pollutant emissions, mostly $SO_2$ and $NO_x$, which according to the World Health Organization (WHO), are hazardous atmospheric pollutants. Some consequences at different scales are caused by these harmful gases: intensification of the greenhouse effect, acid rain, and public health problems. More than 90% of the world population lives in places where the concentrations of pollutants exceed their limits, according to

 doi:10.20944/preprints202009.0398.v1

WHO. The WHO also estimates that 4.2 million people die every year only due to air pollution [5]. In developed countries, low emission zones limit the circulation in urban centers of transport that mainly requires diesel. The United Nations (UN), for example, discusses the issue of environmental pollution since 1972 at the Stockholm Conference in Sweden, and until more recently at COP 25 in Madrid, Spain, in 2019. Currently, the world population suffers from the pandemic outbreak caused by Covid-19, resulting in respiratory diseases. Recent investigations show that the primary victims are older people and/or people with respiratory problems presented before the contamination [6–9]. The indispensable urgency for the reduction of air pollutants is clear from different scales and needs. As such, the introduction of semiconductor nanoparticles into asphalt mixtures can make part of the solutions available to mitigate air-quality problems [10–16].

It is estimated that 40% of urban areas are covered by pavements due to the rapid human development, affecting the local ecosystems and the subjacent surface conditions. Nowadays, another urban problem is the UHI phenomenon, which is the increase of temperatures in cities in comparison to the colder conditions of suburban zones and rural areas, due to the massive development of urbanization [4,17]. Traditional (asphalt) pavements and roofs absorb and store most of the solar energy during the day, which is released in the form of heat during the night. The dark surfaces of, for example, the asphalt pavements, are characterized by a sunlight reflection up to only 20%. Therefore, light-colored road pavements can be considered a viable technology to tackle this phenomenon. Besides, these surfaces reduce the heat convection from pavement to air with a consequent decrease of ambient air temperature. Its high reflectivity reduces the overheating during the summer period, resulting in fewer distresses and increasing pavement durability [2,3].

A common practice to separate asphalt binder fractions is to fractionate it based on polarity using different solvents. By this method, the following fractions are obtained: asphaltenes, resins, aromatics, saturates with decreasing polarity order [18]. To obtain light-colored asphalt pavements, transparent binders can be used. Thus, they are produced through three different processes: i) bitumen modification based on the extraction of asphaltenes that are responsible for the black color of bitumen; ii) synthetic binder production by transparent polymer materials, and iii) blending specific resins with bio-oils or organic vegetal origin materials [2,3]. Even though they are not bituminous materials, their rheological properties are similar to asphalt bitumens [3]. They can even contribute to electricity cost savings (and reduced pollutant emissions) due to the increased visibility in dark areas, for example, in tunnels, and, consequently, a reduced need for lighting [3].

There are some specific uses on the application of light-colored binders for the composition of road pavements [19]: i) tunnels; ii) traffic calming areas; iii) car parks; iv) bus lanes; and v) cycle paths. With its use, there are some advantages, for example, safety improvements with better lighting in tunnels and improved demarcation and hazard perception. In parallel, there are some economic benefits with significant savings in energy consumption through reduced lighting costs and also by reducing the surface temperature, potentially leading to lower life cycle costs and longer service intervals [2,20].

Hitherto, little research has been focused on the physicochemical and rheological properties of light-colored binders. Also, the use of $TiO_2$ can bring two benefits in this sense besides environmental effects: i) the functionalization by providing photocatalytic capability can contribute to the environmental remediation; ii) development of lighter asphalt mixture, e.g., from dark brown to light yellow, depending on the used granulates, which can mitigate the UHI.

Bocci et al. (2012) produced a light-colored asphalt mixture with conventional aggregates, lime filler, light-colored binder, and $TiO_2$ powder (1% by aggregate weight). They present the chromatic difference of a tunnel before and after the application of the light-colored asphalt pavement. The coefficient of reflection related to night visibility and the luminance of this technology were respectively 900% and 528% higher than the conventional asphalt mixture. Its stiffness, measured by indirect tensile stiffness (ITS) modulus at 20 °C, was 4039 MPa, which is comparable to conventional asphalt mixtures. Besides, following the Cantabro test, they concluded that the behavior of light-colored asphalt mixture seemed unaffected by the damaging action of water with a weight loss of only 5.4% and 7% for dry and wet conditions, respectively [3].

Preprints (www.preprints.org) | NOT PEER-REVIEWED | Posted: 17 September 2020 doi:10.20944/preprints202009.0398.v1

Bocci E. and Bocci M. (2014) have continued their research about light-colored asphalt mixtures. Light-colored dense-graded mixtures showed about 50% higher Indirect Tensile Strength (ITS) values than traditional black asphalt mixture. They also experienced about 10.0% lower skid resistance than the conventional one. Moreover, the reflectance was at least three times higher than the traditional asphalt mixture [21].

Sengoz et al. (2017) investigated the rheological properties of transparent binder in comparison to a traditional black bitumen [2]. They showed that the penetration, softening point, and dynamic viscosity (at 135 °C) was 55 $10^{-1}$ mm, 56 °C and 788 cP, respectively, for the transparent binder. The traditional black bitumen resisted to fatigue cracking until 22 °C, whereas the transparent binder did until 19 °C. The transparent binder presented higher zero shear viscosity value, that is, higher resistance to permanent deformation under long-term loading when compared to the traditional black bitumen. For the multiple stress creep recovery test, the transparent binder indicated higher R% values (27.6% and 16.6% for 100 Pa and 3200 Pa, respectively) as compared to the traditional binder (2.3% and 0.9% for 100 Pa and 3200 Pa, respectively) [2].

The main objective of this research is to analyze the physicochemical and rheological properties of a transparent binder modified with nano-$TiO_2$ (0.5%, 3.0%, 6.0%, and 10.0%) for the understanding of its limitations and definition of suitable destinations. For this, its physical (conventional), rheological, and chemical properties were assessed and compared to those of a conventional asphalt binder and a commercial PMB.

## 2. Materials

### *2.1. Binders*

In this research, the transparent binder Kromatis 50/70 from Total was used. According to the supplier, this light-colored synthetic binder presents properties similar to other bitumens. It is produced with hydrocarbon resins and low content of asphaltenes, which are removed and replaced by new elastomeric polymers [22].

A conventional 50/70 bitumen and a polymer modified binder (PMB) (SBS-modified bitumen) were also used in this study. These reference binders were named as N50/70 and PMBTS, respectively.

### *2.2. $TiO_2$ nanoparticles*

The semiconductor selected to provide multifunctional properties was the nano-$TiO_2$ by Quimidroga (Aeroxide $TiO_2$ P25). Its main properties are 80% anatase and 20% rutile crystalline phases, purity > 99.5%, and particle size of about 23 to 28 nm.

### *2.3. Sample Preparation*

The nanoparticles were incorporated into the binder (at 150°C for 30 minutes in a low shear mixer with a rotational speed of 1500 RPM) with four different contents: 0.5, 3.0, 6.0 and 10.0% (in the mass of the binder). The samples were named by the modification content: 0.5%, 3.0%, 6.0% and 10.0%. With the introduction of nano-$TiO_2$, the color of the binder changes from dark brown (0%) to light yellow (10.0%), see Fig. 1. One blend was prepared for each content. Regarding the performed tests, the number of replicates respected the requirements mentioned in the relevant European standard.

Preprints (www.preprints.org) | NOT PEER-REVIEWED | Posted: 17 September 2020 doi:10.20944/preprints202009.0398.v1

## 3. Methods

Different tests were carried out, such as penetration, softening point, Dynamic Shear Rheometer (DSR) tests (complex modulus, Linear Amplitude Sweep – LAS, Multiple Stress Creep Recovery - MSCR), Dynamic viscosity and Fourier Transform Infrared (FTIR) spectroscopy, in order to determine conventional, rheological and chemical properties. Fig. 1 presents the schematic summary of the preparation and characterization methodology adopted in this paper.

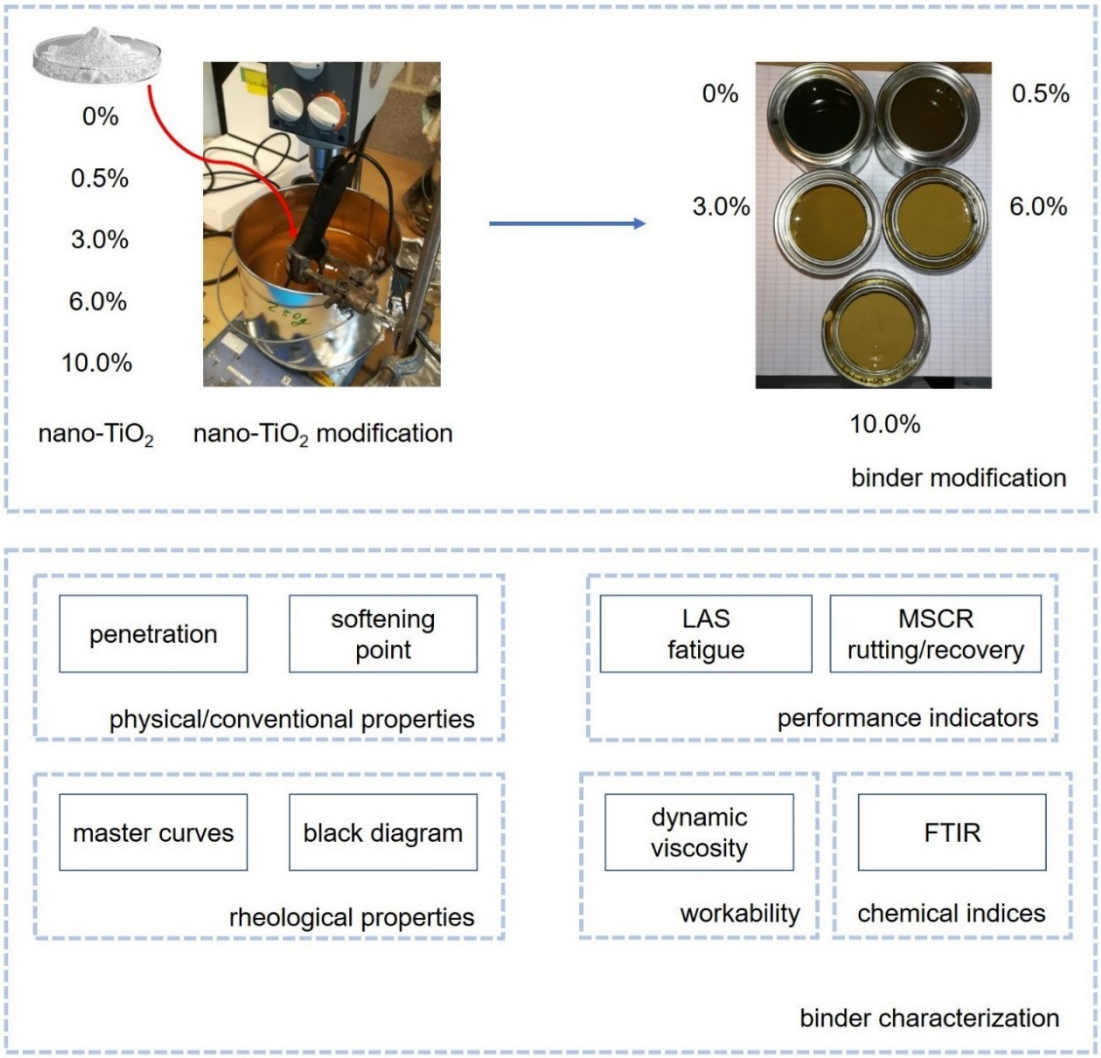


**Figure 1.** Schematic representation of this research.

### *3.1. Penetration and Softening Point*

Penetration and softening point were tested according to EN 1426/2015 and EN 1427/2015, respectively. They indicate the basic properties of asphalt binders.

### *3.2. Dynamic Viscosity*

A dynamic viscosity test was carried out following the EN 13302/2010 standard, but only for the transparent binders (with and without nano-$TiO_2$). The objective was to evaluate the workability of the binders according to Superpave specifications. The highest allowed viscosity to respect the workability is $3\times10^3$ cP (or 3 Pa.s) at 135 °C [23,24].

Preprints (www.preprints.org) | NOT PEER-REVIEWED | Posted: 17 September 2020 doi:10.20944/preprints202009.0398.v1

*3.3. Viscoelastic Behavior*

The viscoelastic behavior of the binders was assessed using the Dynamic Shear Rheometer (DSR). The DSR used in this study is an Anton Paar MCR 500. For the temperature ranges from 0 °C to + 40 °C and from + 40 °C to + 80 °C, the 8 mm and 25 mm plate geometries were used accordingly as described in EN 14770:2012. For each temperature step (increments of 10 °C), frequency sweep tests were performed (0.1-10 Hz) on two replicates per binder sample, within the linear viscoelastic region (LVER) of the binders. The data were further analyzed using the RHEA™ software [25]. The shifting of the data was performed using the Gordon and Shaw procedure [26]. The phase angle and complex modulus master curves are presented in their original format, without fitting any mathematical or mechanical models.

Black diagrams (complex modulus versus phase angle) aim to identify discrepancies of the rheological data, breakdown of time-temperature equivalence, and thermo-rheological simplicity [27]. A smooth curve indicates time-temperature equivalence, a typical response of unmodified binders. On the other hand, discontinuities indicate the presence of high wax content bitumen, highly polymer modified bitumen, or a highly asphaltene structured binder [27]. Also, it is possible to notice whether there are different dominances when the binder is a composite [27]. This phenomenon happens, for example, when the complex modulus trend changes with the increase of the phase angle, a phenomenon known as curling.

*3.4. Fatigue resistance (LAS test)*

In order to evaluate the fatigue resistance of bituminous binders, the Linear Amplitude Sweep (LAS) test was performed. This test is an accelerated method that uses the DSR (8 mm parallel plate geometry at 15 °C), which consists of two steps: i) firstly frequency sweep test, and ii) secondly amplitude sweep test, as described in AASHTO TP 101-14. The frequency sweep test (0.2-30 Hz) is used to define the undamaged properties and fatigue law parameters, at a strain level of 0.1%. A linear amplitude sweep test is performed at 10 Hz, and the strain amplitude is linearly increased during 3000 cycles, from 1% to 30%. The Viscoelastic Continuum Damage (VECD) theory is used to determine the parameters A and B of the fatigue law (Eq.1) [28], in order to determine the fatigue life (Nf). The failure point is determined as the point when the product of the complex modulus (G*) and phase angle (δ) sine is reduced by 35% from its initial value.

$$Nf = A\,\gamma^{B} \quad (1)$$

Both the fatigue curves and the Nf for strain levels ($\gamma$) equal to 2.5% and 5%, related to a strong and weak pavement [29], respectively, will be presented.

*3.5. Rutting resistance indicator (MSCR test)*

The Multiple Stress Creep Recovery (MSCR) was performed using the DSR together with the 25 mm plate and 1 mm gap, as described in EN 16659:2015. The test is performed at 50 °C, at two different stress levels (0.1 and 3.2 kPa) during ten load cycles. Each cycle consists of 1 s loading followed by 9 s of a recovery period, from which two parameters are obtained: i) the non-recoverable creep compliance Jnr ($Pa^{-1}$), which is the ratio between the residual strain and the stress applied; and ii) the recovery R (%), showing proportionally how much strain the sample recovers at the end of the cycle. R (%) can be used to identify the presence of polymer modifications in the asphalt binders.

*3.6. FTIR*

Chemical characterization of binders has received attention in the literature as it can present functional groups related to the crude oil origin, the polymer modification, and the degree of oxidation [30–35]. Since this paper aims to analyze the chemical characteristics of the transparent binder modified with nano-$TiO_2$, three approaches were carried out: i) identification of FTIR peaks; ii) establishment of a possible relationship between the $TiO_2$ modification level and related chemical groups; and iii) comparison of standard indices with reference binders used in this study.

Preprints (www.preprints.org) | NOT PEER-REVIEWED | Posted: 17 September 2020 doi:10.20944/preprints202009.0398.v1

The Thermo Scientific Nicolet iS10 Fourier Transform Infrared (FTIR) spectrometer is equipped with an Attenuated Total Reflectance (ATR) fixture and a Smart Orbit Sampling Accessory. The average spectra were obtained after the acquisition of the spectra, 32 repetitive scans in the range 400 $cm^{-1}$ to 4000 $cm^{-1}$ with a resolution of 4 $cm^{-1}$ were performed to deliver an average spectrum. A hot droplet of each binder was placed on the crystal, and its respective spectrum was measured.

The chemical structure of the binders was analyzed using indices, *I*, from the obtained FTIR spectrum [36]. Each *I* (Eq. 2) is calculated by the ratio of the peak area of the identified band by the total area (Eq. 3) of the spectrum.

$$I_{Functional\ Group} = \frac{A_i}{\Sigma A} \quad (2)$$

$$\Sigma A = A_{1700} + A_{1600} + A_{1460} + A_{1376} + A_{1030} + A_{864} + A_{818} + A_{743} + A_{724} + A_{(2953,\ 2923,\ 2862)} \quad (3)$$

Where $Ai\ is$ the peak area of the specific functional group.

The areas defined by the introduced baselines and the part of the spectrum were calculated using a specific software Origin. Each peak is attributed to a functional group remaining unaffected during service life, but also to groups responsible for aging or polymer presence [30,32]. When it comes to the groups responsible for $TiO_2$, echoing [37–39] in the region below 1000 $cm^{-1}$, several peaks are ascribed to $TiO_2$ presence. Previous researchers have demonstrated that the peak around 657 $cm^{-1}$ is attributed to Ti-O-Ti stretching vibration, whereas the peak around 590 $cm^{-1}$ is due to the vibration of Ti-O-O. A broader band of wavenumbers was calculated around these peaks in order to capture their increase by elevating the $TiO_2$ modification level. It should be noted that a horizontal baseline coinciding with the X-axis was used for the calculation of this area. RI (Eq. 4) was calculated in order to check the relative increase of $TiO_2$ modification. $I_{TI-O+Ti-O-O}$ is the index of each binder, and $I_{TI-O+Ti-O-O0\%}$ is the index of the transparent base binder (0%).

$$RI = \frac{I_{TI-O+Ti-O-O} - I_{TI-O+Ti-O-O0\%}}{I_{TI-O+Ti-O-O0\%}} \% \quad (4)$$

More specifically for asphalt binders, the sulfoxide, carbonyl, aromatic, aliphatic, branched aliphatic, long chains, polybutadiene, and polystyrene indices were calculated. Sulfoxide and carbonyl indices are both related to aging.

They were calculated considering the following method: i) aromatic index: $A_{1600}/\Sigma A$; ii) aliphatic index: $(A_{1460} + A_{1376})/\Sigma A$; iii) branched index: $A_{1360}/(A_{1460} + A_{1376})$; iv) long chain index: $A_{724}/(A_{1460} + A_{1376})$; v) carbonyl index: $A_{1700}/\Sigma A$; vi) sulphoxide index: $A_{1030}/\Sigma A$; vii) polybutadiene index: $A_{966}/\Sigma A$; and viii) polystyrene index: $A_{699}/\Sigma A$.

Aromatic, aliphatic, branched aliphatic, and long chains are the structural groups of asphalt binders. Polybutadiene and polystyrene are associated with SBS modified binders. For details concerning the determination of standard indices related to oxidative aging of the binder, the reader is referred to the protocol described in [36]. Briefly, a common practice in this processing method is to introduce tangential baselines defined by limits around certain peaks [40].

## 4. Results and Discussions

### *4.1. Penetration and Softening Point*

Figs. 2 and 3 show the resulted penetration and softening point of the studied binders. When compared to the transparent base binder, the inclusion of 0.5%, 3.0% and 6.0% $TiO_2$ nano-modification decreased the penetration from 49 to 47, 45, and $47\times10^{-1}$ mm, respectively. For 10.0% $TiO_2$, it increased to $53\times10^{-1}$ mm, being similar to the N50/70 results. When compared to the PMBTS,

Preprints (www.preprints.org) | NOT PEER-REVIEWED | Posted: 17 September 2020 doi:10.20944/preprints202009.0398.v1

all the penetration results were higher. So, the penetration values of the Kromatis binder were between the conventional and the PMB binders.

For the softening point, the results of the transparent binders were around 59 °C. The increase of the $TiO_2$ content gradually increased the softening point by about 4 °C. The transparent binders had a softening point again between the ones of the conventional and the PMB binders.

Comparing these results to those obtained by Sengoz et al. (2017) for the same binder from the same supplier, they showed that the penetration and softening points were $55\times10^{-1}$ mm and 56°C [2]. Thus, here in this research, the transparent base binder had a lower penetration but a higher softening point [2].

It can be concluded that the transparent binders had results between the conventional and the PMB binders but more similar to the conventional one. The incorporation of nano-$TiO_2$ gradually increased the softening point. For the penetration, the results were lower until 6.0%, but higher for 10.0%.

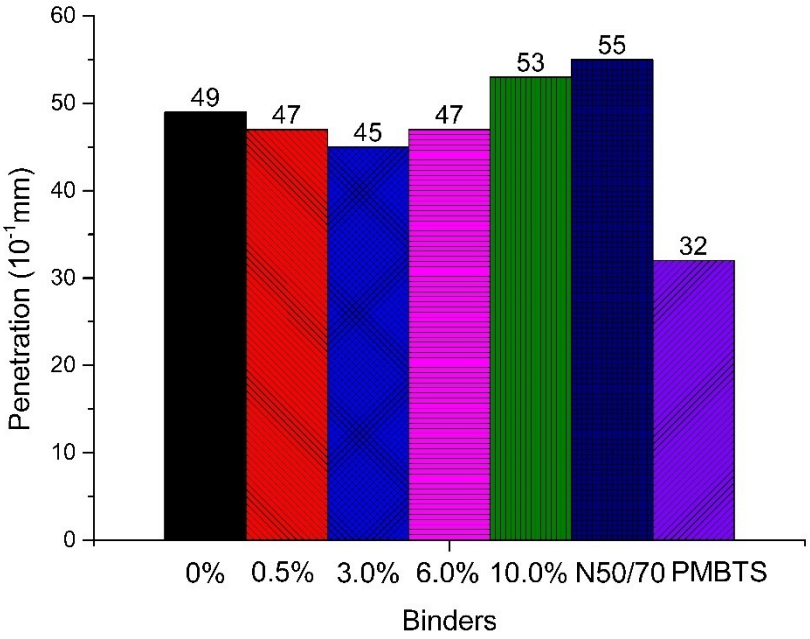


**Figure 2.** Penetration results of the binders of this study.

Preprints (www.preprints.org) | NOT PEER-REVIEWED | Posted: 17 September 2020 doi:10.20944/preprints202009.0398.v1

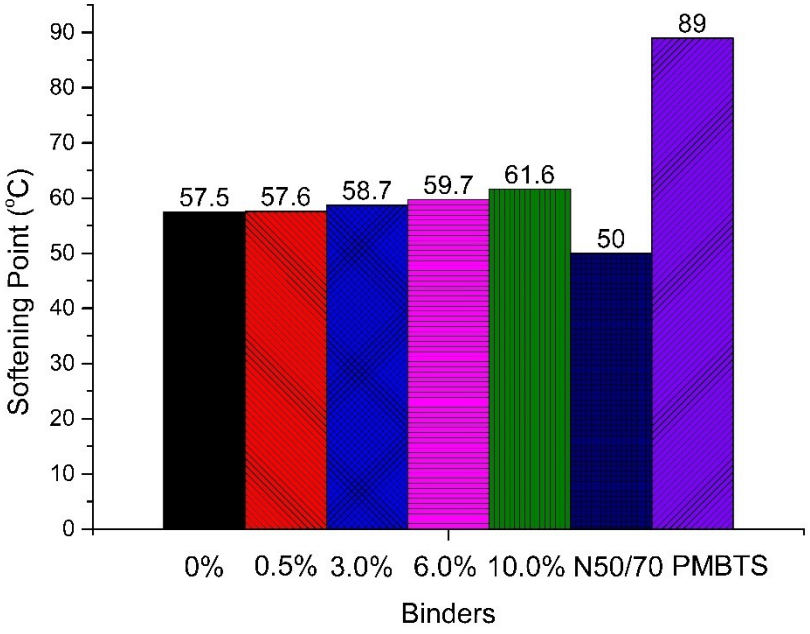


**Figure 3.** Softening point results of the binders of this study.

*4.2. Dynamic Viscosity*

The dynamic viscosity, carried out only for the transparent binders, is shown in Fig. 4. The introduction of nano-$TiO_2$ increased dynamic viscosity. At 135 °C, the viscosity increased from $1\times10^3$ cP (for the base binder) to $2.3\times10^3$ cP (for the 10.0%). Also, all the binders had a viscosity lower than $3\times10^3$ cP, considered as the recommended maximum viscosity criterion under Superpave to guarantee proper binder pumping in the asphalt plant during production [41]. If this value is higher than $3\times10^3$ cP, excessive energy is needed for the mixing and compaction of asphalt mixtures [23]. It can be concluded that all the modified transparent binders using the contents of nano-$TiO_2$ studied (from 0 to 10.0%) are feasible considering their workability. It is also interesting that the 10.0% $TiO_2$ appears to have the highest energy requirements as its viscosity is close to the Superpave threshold. Thus, from an economic point of view, it would be favorable to target for lower $TiO_2$ levels.

In addition, the comparison of the results to those from the literature reveals that a higher viscosity was reached ($1\times10^3$ cP). For example, Sengoz et al. (2017) presented 788 cP in dynamic viscosity for the same transparent binder [2].

Preprints (www.preprints.org) | NOT PEER-REVIEWED | Posted: 17 September 2020 doi:10.20944/preprints202009.0398.v1

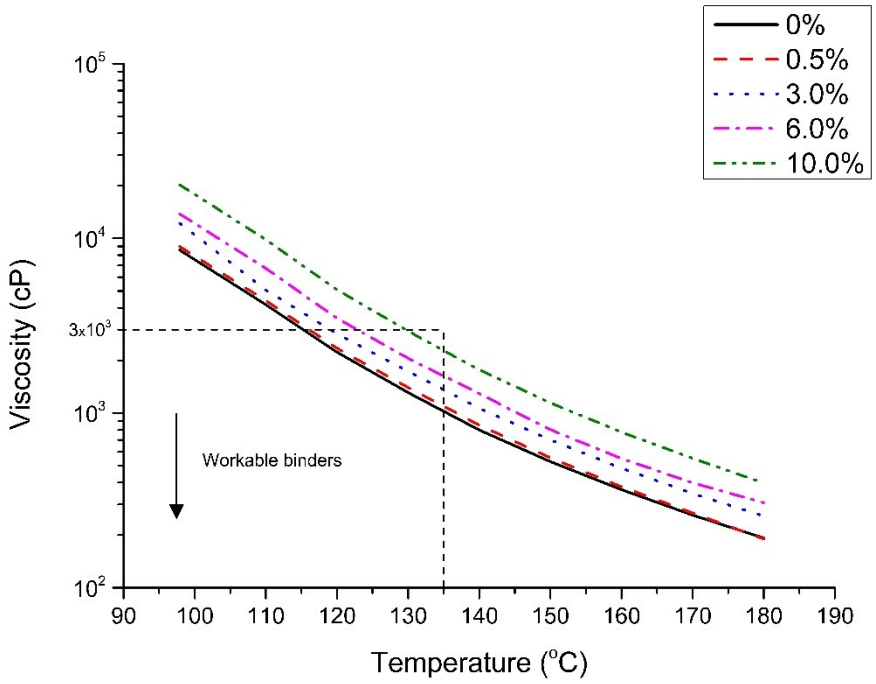


**Figure 4.** Dynamic viscosity results of the binders of this study.

*4.3. Viscoelastic behavior*

The complex modulus and phase angle master curves are presented in Fig. 5. The addition of $TiO_2$ slightly alters the viscoelastic behavior of the transparent binder, leading to a simultaneous small increase of modulus and a decrease of the phase angle. The N50/70 shows a simple viscoelastic behavior with the phase angle gradually approaching the viscous asymptote of 90° at elevated temperatures, a typical response of an unmodified binder. Concerning the complex modulus, the N50/70 shows similar values to the PMBTS at frequencies above 10 Hz. At low frequencies (related to high temperature), N50/70 shows the lowest complex modulus compared to other binders, which was an expected observation since the modulus of those binders is greatly influenced by the polymer modification.

Comparing the transparent binder with the PMBTS, it can be seen that the complex modulus is similar at lower frequencies, while the PMBTS demonstrates a lower modulus at frequencies above 0.01 Hz. Looking at the phase angle, both reveal the presence of elastomeric modification, which is visible by the drop of the phase angle at a low reduced frequency. For the PMBTS, the dominance of the polymeric phase starts below 1 Hz and shows at a steady plateau stage of 60°. On the other hand, the dominance of the polymeric phase for the transparent binders starts after 0.01 Hz (which can be translated that the polymer network is "active" at higher temperatures compared to the PMBTS) showing a significant drop of the phase angle and then gradually approaching the viscous asymptote of 90°.

The last part shows that the polymer network is no longer dominant. Those distinct differences can be attributed to the difference between the base binders as well as the compatibility between base and polymer [42]. Another possibility is the thermal history of the binders, which can significantly

Preprints (www.preprints.org) | NOT PEER-REVIEWED | Posted: 17 September 2020 doi:10.20944/preprints202009.0398.v1

influence the rheological behavior of elastomeric binders, as demonstrated by Soenen et al. [43].

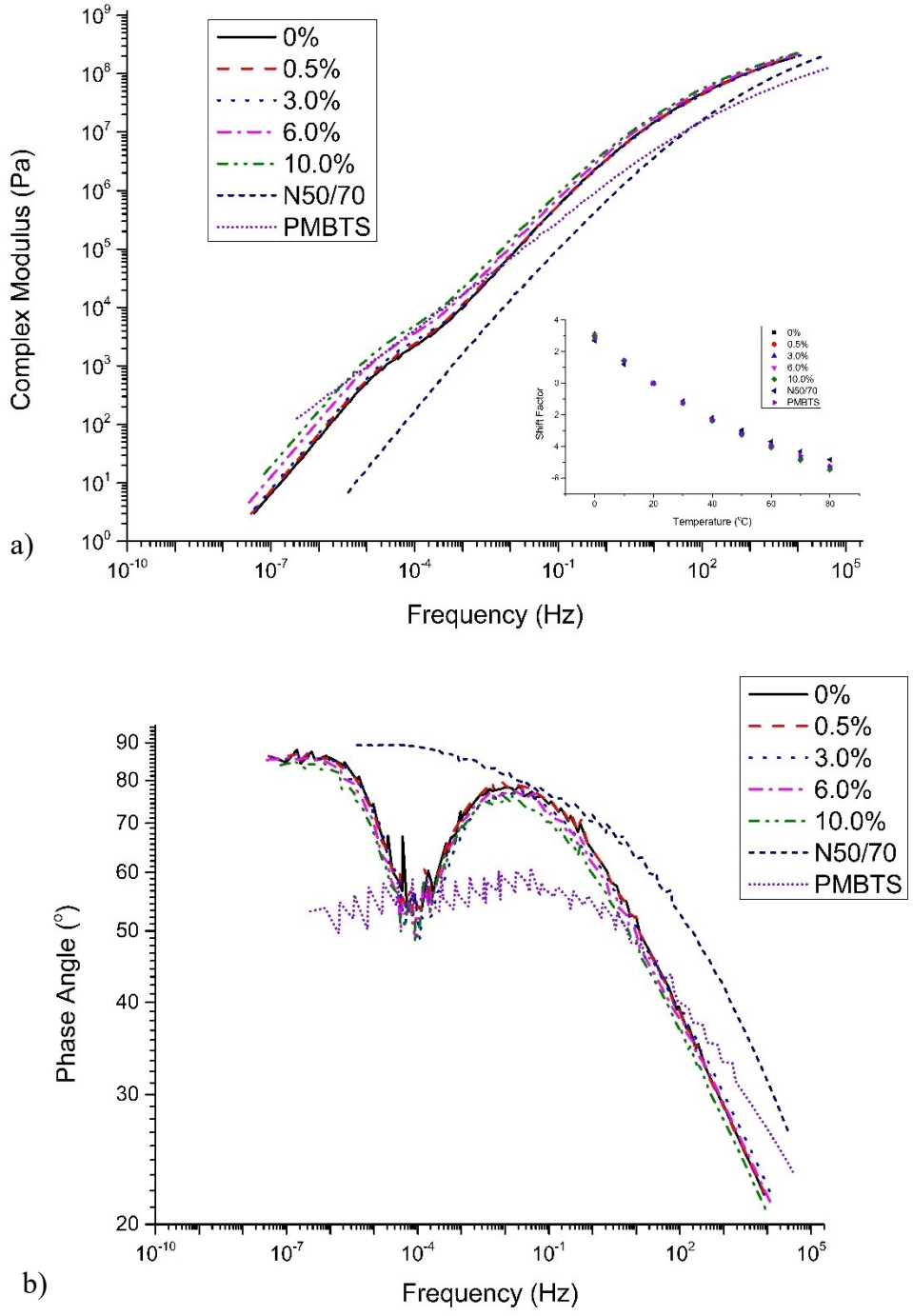


**Figure 5. a)** Complex modulus and **b)** phase angle master curves of the binders of this study

The black diagram (Fig. 6) shows the combined effect of complex modulus and phase angle for the different binders. The N50/70 binder presents a conventional black diagram curve. Therefore, it is smooth, and the complex modulus decreases while the phase angle increases. The presence of a polymer can be seen by the shift of the curve towards a lower phase angle (higher elastic behavior) [27]. More specifically, for the PMBTS, the plateau near 60° (at a temperature of 58 °C) can indicate that the polymer forms a continuous elastic network when dissolved in bitumen, making it a polymer-dominant phase.

Preprints (www.preprints.org) | NOT PEER-REVIEWED | Posted: 17 September 2020 doi:10.20944/preprints202009.0398.v1

The shape of the curve of the transparent binders is different from the reference ones showing three distinctive regions: i) from $10^8$ to $5\times10^5$ Pa, the complex modulus decreases with the increase of the phase angle; ii) from $5\times10^5$ to $5\times10^4$ Pa: the complex modulus decreases when the phase angle increases; and iii) from $5\times10^4$ Pa with the same pattern of the first region, including the shape. This viscoelastic response indicates an alternation of dominance between the materials that compose the transparent binders, as also observed in the phase angle master curve. Besides, transparent binders seem to be more elastic than N50/70, with a partial shift towards the left. The addition of $TiO_2$ seems to have a small, rather insignificant, effect on the viscoelasticity of the transparent binder. Based on the observations of the master curves and black diagram, the addition of $TiO_2$ up to 10.0% seems to not introduce any noticeable effect on the structure of the transparent binders.

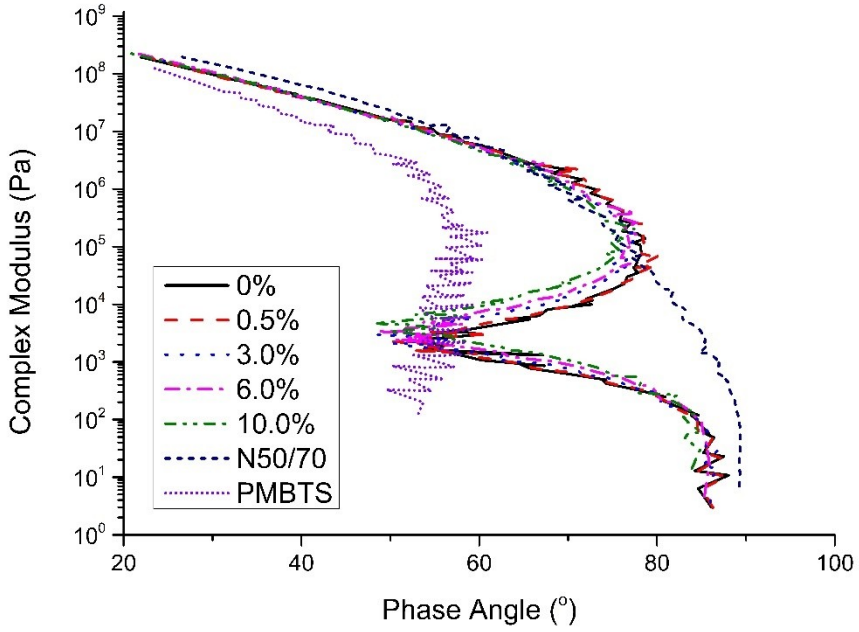


**Figure 6.** Black diagram of the evaluated reference and transparent binders

*4.4. Fatigue resistance (LAS test)*

The fatigue curves of each binder are presented in Fig. 7 and the corresponding parameters are further elaborated in Table 1.

The PMBTS shows the highest fatigue resistance among the binder samples, while the transparent base binder and the N50/70 showed similar results. The addition of $TiO_2$ seems to harm the fatigue life of the transparent binder, except for the 0.5% dosage, where it shows a slightly improved fatigue life. In more detail, the addition of $TiO_2$ leads to a proportional decrease of the slope (parameter B), while no clear trend is evident on the effect of $TiO_2$ on the intercept (parameter A).

For all the binders, from the lowest to the highest fatigue performance considering the applied strain of 2.5% (representative strain level of a "weak" pavement structure), the progressive sequence is 10.0%<6.0%<N50/70<3.0%<0%<0.5%<PMBTS. For the applied strain of 5% (representative strain level of a "strong" pavement structure), the progressive sequence is 10.0%<6.0%<3.0%<N50/70<0%<0.5%<PMBTS. High contents of nano-$TiO_2$ slightly reduced the binder fatigue resistance. Besides, the higher differences are found for an applied strain level of 5%, related to the strong pavement structures.

Preprints (www.preprints.org) | NOT PEER-REVIEWED | Posted: 17 September 2020 doi:10.20944/preprints202009.0398.v1

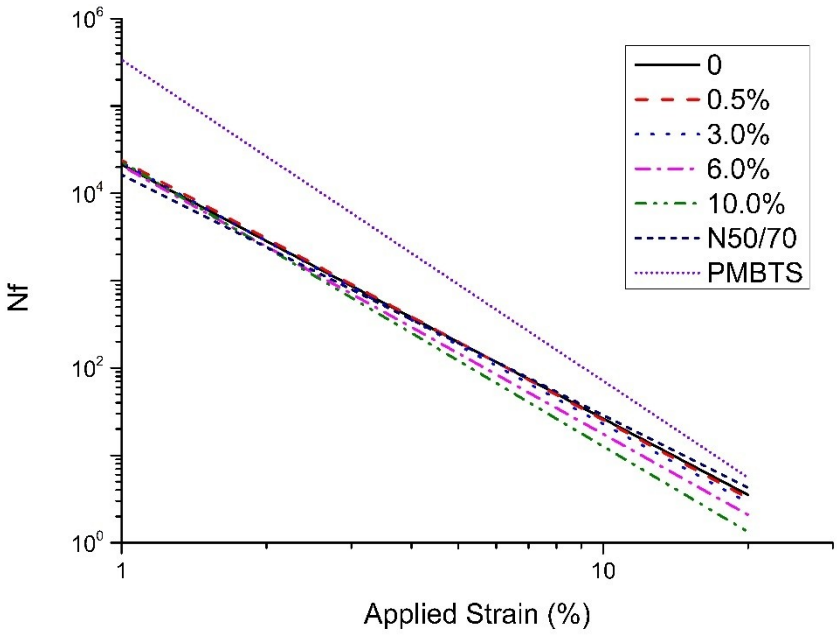


**Figure 7.** LAS Test: Nf versus applied strain

**Table 1.** LAS test results.

| Binder | Parameter | | | |
|---|---|---|---|---|
| | A | B | Nf 2.5% | Nf 5% |
| 0% | 21348 | -2.9 | 1486 | 198 |
| 0.5% | 23946 | -3.0 | 1568 | 199 |
| 3.0% | 22578 | -3.0 | 1453 | 182 |
| 6.0% | 20724 | -3.1 | 1241 | 148 |
| 10.0% | 22942 | -3.3 | 1160 | 121 |
| N50/70 | 16303 | -2.8 | 1308 | 194 |
| PMBTS | 338013 | -3.7 | 11631 | 909 |

*4.5. Rutting resistance indicator (MSCR test)*

The MSCR test has been introduced as a test to evaluate the resistance to permanent deformation (rutting) as well as a tool to evaluate the quality of polymer modified binders [44,45]. Generally, a combination of high recovery (R) and low non-recoverable compliance ($J_{nr}$) indicates a good quality PMB that can be utilized in high traffic pavements, as described in AASHTO M332. Such limits that distinguish between the acceptance levels for different traffic levels have not been established by the EN 16659. Therefore, a comparative evaluation of the rutting resistance of the binders in this study is presented.

The MSCR test results are presented in Table 2. Considering the %R, the transparent binders exhibit a recovery between the reference binders (higher than N50/70 but lower than PMBTS), but with values closer to PMBTS. At a stress level of 100 Pa, while the conventional binder N50/70 demonstrates recovery of only 9.0%, the transparent binders show at least 63.6% and the PMBTS 82.1%.

The incorporation of nano-$TiO_2$ increased the R100 for the contents 6.0% and 10.0% when compared to 0%. The contents 0.5% and 3.0% had similar R100 to 0%. For R3200, the transparent binders had similar results, from 63.2% to 65.8%, for 0% and 10.0% $TiO_2$ addition respectively.

Preprints (www.preprints.org) | NOT PEER-REVIEWED | Posted: 17 September 2020 doi:10.20944/preprints202009.0398.v1

Regarding the Jnr values, again, the transparent binders show an intermediate behavior between the reference binders N50/70 and PMBTS. The incorporation of nano-$TiO_2$ decreased the Jnr (100 and 3200 $Pa^{-1}$) for the contents 3.0%, 6.0% and 10.0% when compared to 0%. As can be expected, the content 0.5% had a similar Jnr to 0% (transparent base binder).

Sengoz et al. (2017) analyzed the same Kromatis 50/70 from the same supplier. They indicated values of R% between the N50/70 and PMBTS as well, 27.6% and 16.6% for 100 Pa and 3200 Pa, respectively [2]. Nevertheless, their results are closer to the N50/70 than the PMBTS. Considering Jnr, the results from Sengoz et al. (2017) are much higher than those obtained in this research for all the binders (base, modified, and reference ones).

**Table 2.** MSCR test results.

| Binder | Parameter | | | |
|---|---|---|---|---|
| | **Jnr,100 ($kPa^{-1}$)** | **Jnr,3200 ($kPa^{-1}$)** | **R100 (%)** | **R3200 (%)** |
| 0% | 0.2 | 0.2 | 64.8 | 63.2 |
| 0.5% | 0.2 | 0.2 | 63.6 | 62.3 |
| 3.0% | 0.2 | 0.2 | 65.5 | 63.8 |
| 6.0% | 0.1 | 0.1 | 69.9 | 64.4 |
| 10.0% | 0.1 | 0.1 | 73.1 | 65.8 |
| N50/70 | 0.6 | 0.6 | 9.0 | 6.0 |
| PMBTS | 0.0 | 0.0 | 82.1 | 85.7 |
| Kromatis 50/70 from [2] | 1.8 | 2.3 | 27.6 | 16.6 |

It can be concluded that the transparent binders present better rutting resistance than the conventional N50/70 with higher recovery and lower non-recoverable creep compliance. This fact was expected since the transparent binder contains elastomeric polymers, as demonstrated earlier in section 4.3. However, the transparent binders presented lower rutting resistance than the PMBTS. The incorporation of nano-$TiO_2$ can increase the rutting resistance for high contents (mainly 6.0% and 10.0%).

### *4.6. FTIR*

#### 4.6.1. Peak identification

The FTIR spectra (absorbance versus wavelength) of the ($TiO_2$-modified) transparent binders, the reference binders, and the pure $TiO_2$ are shown in Fig 8. Peaks at 2953 $cm^{-1}$ and 2862 $cm^{-1}$ are associated with stretching vibrations of $sp^3$ C–H in aliphatic chains, asymmetric and symmetric stretches, respectively. Peaks at 1460 $cm^{-1}$ are characteristics of bending vibrations of methylene groups (-$(CH_2)_n$). The peak at 1375 $cm^{-1}$ is attributed to the bending of methyl groups (-$CH_3$), which is related to aliphatic branched bands. The long-chains band can be seen at 724 $cm^{-1}$, associated with the rocking motion of -$CH_2$ groups in an aliphatic chain. The peak at 1700 $cm^{-1}$ is related to the stretching of carbonyl band C=O typical of carboxylic acids, being one of the most important peaks for the asphalt binder aging [46–48].

Stretching absorptions of C=C bond in aromatic rings occur at the peaks at 1600 $cm^{-1}$. The peaks that appear between 910 $cm^{-1}$ and 699 $cm^{-1}$ can be analyzed carefully to show ortho-, meta- and para-disubstituted rings presented in aromatic compounds and are associated with out-of-plane C-H bending vibrations in this structure. Due to the complex composition of the asphalt binders, all these compounds may be presented in the analyzed samples. For example, the pair 743 $cm^{-1}$ and 699 $cm^{-1}$ can match with monosubstituted rings; a single peak at 743 $cm^{-1}$ may be associated to 1,2-

Preprints (www.preprints.org) | NOT PEER-REVIEWED | Posted: 17 September 2020 doi:10.20944/preprints202009.0398.v1

disubstituted rings; peaks at 864 $cm^{-1}$, 783 $cm^{-1}$, and 699 $cm^{-1}$ may be attributed to 1,3- disubstituted rings and finally the pair 864 $cm^{-1}$ and 814 $cm^{-1}$ can match to 1,4-disubstituted rings [46–48].

The peaks at 966 $cm^{-1}$ and 699 $cm^{-1}$ may still correspond to the bending out-of-plane of C-H of trans-alkenes (from polybutadiene) and C-H out-of-plane bending in monoalkylated aromatics (from polystyrene) associated with SBS. The peak at 910 $cm^{-1}$ can also show terminal-alkenes [46]. The peak at 1375 $cm^{-1}$ may be associated with the asymmetric stretch of sulfonyl chlorides S=O bond. While the peaks at 1310 $cm^{-1}$ and 1152 $cm^{-1}$ are typical of respectively asymmetric and symmetric stretches of sulfones S=O bonds [18]. At 1030$cm^{-1}$, there is the other peak directly related to asphalt binder aging, the stretch of sulfoxide S=O bond [46–48]. The peak 1242 $cm^{-1}$ can be linked to the asymmetric stretching vibration of sulfate esters [18].

For the transparent binders, the peak 434 $cm^{-1}$ represents a stretching vibration of metal oxides (M-O) bond (M can be Si, Mn, V, Ni, and others) [49–52]. This peak (434 $cm^{-1}$) is also attributed to stretch absorptions of Ti-O bond [53], and the increase in this peak area in the $TiO_2$-modified transparent binders may indicate the proper incorporation of the semiconductor in the asphalt binder.

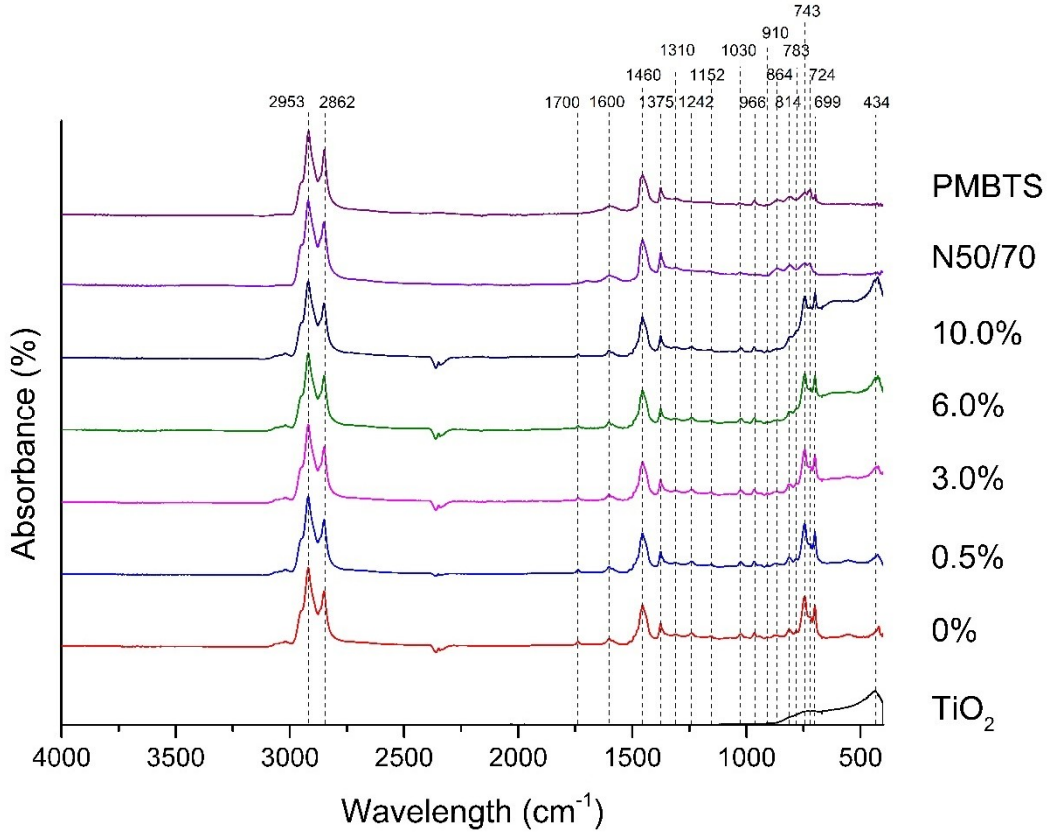


**Figure 8.** FTIR spectra of the binders of this study

4.6.2. Relationship between the TiO2 modification level and chemical responsible

Fig. 9 shows the graph RI versus % $TiO_2$. It can also be seen that the addition of nano-$TiO_2$ increases the relative increase RI (from $TiO_2$ related vibration area). A linear correlation of the nano-$TiO_2$ percentage and the RI can be found. 3To some extent, this shift of the spectra with the addition of nano-$TiO_2$ can be expected as the vibrations become more evident when the binder is more diluted. The high correlation coefficient ($R^2$ = 0.99) of the increase of this index with the modification level (Fig. 9) can confirm the assumption that nano-$TiO_2$ can be used as a marker in bituminous blends [54,55]. This analysis can be used in order to assess the presence of $TiO_2$ and quantify its incorporation as a binder modifier.

Preprints (www.preprints.org) | NOT PEER-REVIEWED | Posted: 17 September 2020 doi:10.20944/preprints202009.0398.v1

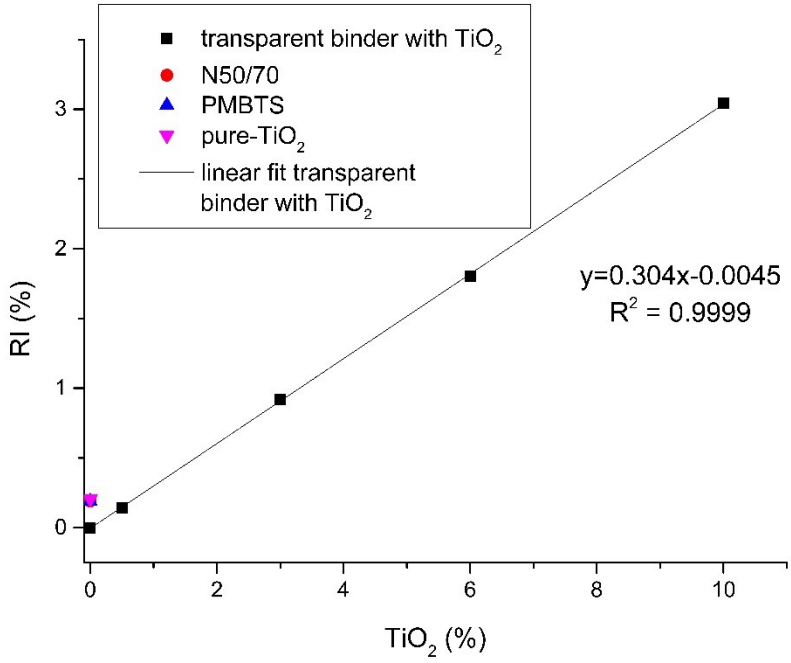


**Figure 9.** Correlation of the nano-TiO2 modification level with the increase of the TiO2-related index.

4.6.3. Relationship between the TiO2 modification level and chemical responsible

The results of FTIR are presented in Fig. 10 in terms of oxygen- and polymer-related indices. The chemical indices sulfoxide, carbonyl, polybutadiene, polystyrene, aromatic, aliphatic, branched aliphatic, and long chains are presented in terms of their normalized intensity. This study confirms that the initial sulfoxide and carbonyl levels of nano-$TiO_2$-modified are similar to the reference unmodified binder N50/70 and the SBS-modified PMBTS. This observation gives rise to the assumption that the presence of nano-$TiO_2$ does not introduce new functionalities in sulfoxide- or carbonyl-related groups such as esters, carboxylic acids, and ketones. Besides that, the modification of the binder with nano-$TiO_2$, according to other studies [56,57], can reduce the long-term oxidation performance due to its capability to reflect and absorb UltraViolet (UV) light during photocatalysis. It is also initially chemically neutral for the polar carbonyl groups.

Preprints (www.preprints.org) | NOT PEER-REVIEWED | Posted: 17 September 2020 doi:10.20944/preprints202009.0398.v1

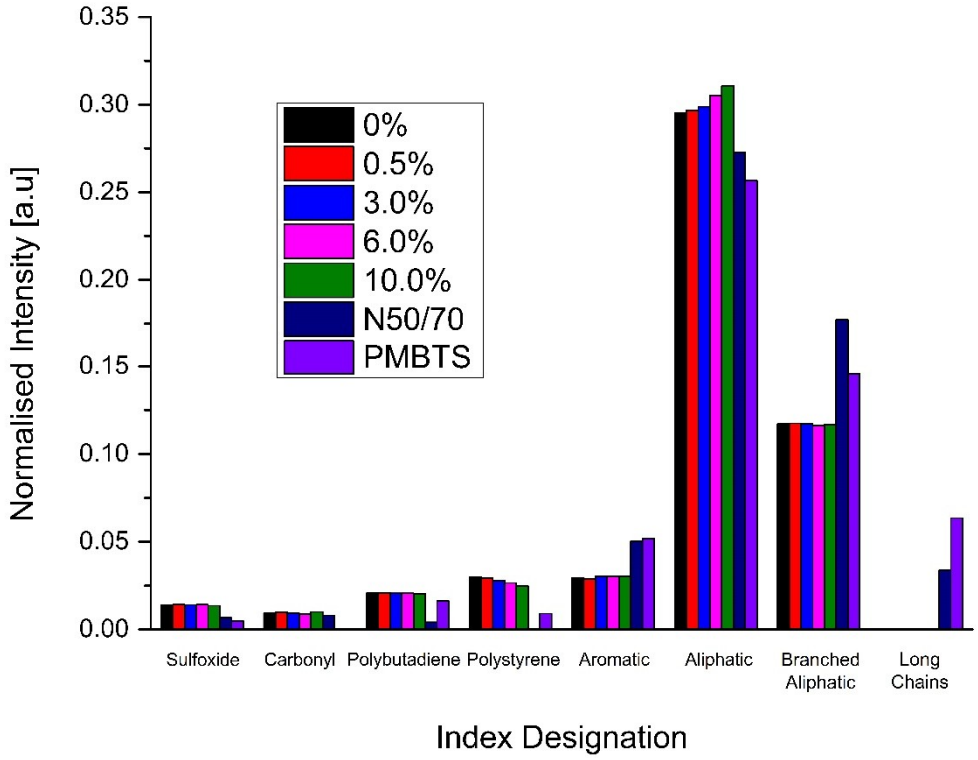


**Figure 10.** FTIR indices of the nano-TiO2-modified, base and reference binders.

A detailed observation of the two aging-related indices implies that, although of similar magnitude, slightly higher indices can be found compared to the two reference binders N50/70 and PMBTS. This fact can be explained as the result of the different initial sulfur content for the sulfoxide index. In other words, the origin of the crude oils of the binders is different, and this has a clear implication to the S=O-containing groups. When examining the slightly higher carbonyl index of the nano-$TiO_2$-modified binders, one can highlight two important points. Firstly, the binder used for modification with nano-$TiO_2$ was different from the unmodified reference binder, and transparent binders show a carbonyl index of the same magnitude. The level of modification seems to have a negligible effect on the initial carbonyl index. That is, the increased carbonyl level can be attributed to the binder utilized as the base for modification and not the nano-$TiO_2$ addition itself. Following the explanation provided for the higher carbonyl increase of nano-$TiO_2$-modified binders, the same line of thought can be followed for the slightly lower aromatic, branched aliphatic, and long chains indices and the higher aliphatic index compared to the reference binders.

In parallel, as the introduction of elastomeric polymers produces the binder selected as the base for $TiO_2$ modification, the polymer-related indices were evaluated. A comparison of the polybutadiene and polystyrene indices reveals that the binder used for modification (transparent base binder) is highly modified compared to the SBS modified reference binder PMBTS. For the binder N50/70, these indices are not applicable.

Different from the rheological parameters, the transparent binders did not show intermediate behavior between the reference binders N50/70 and PMBTS. They showed higher indices for sulfoxides, carbonyl, polybutadiene, polystyrene, and aliphatic but lower for aromatic, branched aliphatic and long chains. Their long chains were null. Moreover, the $TiO_2$ modification seems to have little effect on the indices, except for the polystyrene and aliphatic indices. The polystyrene index decreases, and the aliphatic index increases with the increase of nano-$TiO_2$.

 doi:10.20944/preprints202009.0398.v1

## 5. Conclusions

A transparent binder modified with nano-$TiO_2$ was characterized regarding its physicochemical and rheological properties in this paper. It is useful for specific applications, such as tunnels, calming traffic areas, among others, as the nano-$TiO_2$ provides to the pavement a photocatalytic function and better visibility. Modified transparent binders, with 0.5%, 3.0%, 6.0%, and 10.0% of nano-$TiO_2$, were compared to the transparent base binder and also with two commercial asphalt binders (conventional and PMB). The results of the experimental activity led to the following conclusions:

- For the penetration and softening point, the transparent binders (base and modified) had results between the conventional binder and PMB. When compared to the transparent base, the incorporation of nano-$TiO_2$ gradually increased the softening point and decreased the penetration up to 6.0%.
- Based on the dynamic viscosity, the workability of the $TiO_2$-modified binders is feasible until 10.0% of modification content.
- The modification with nano-$TiO_2$ did not cause substantial changes in the Complex Modulus of the transparent binder. The PMB and transparent binders clearly reveal the presence of an elastomeric modification, which is visible by the drop of the phase angle around the frequency of $10^{-4}$ Hz. There is a discontinuity in their curve, which can be attributed to the difference between the base binders as well as the compatibility between base and polymer or their thermal history.
- The black diagram suggests an alternation of elastic/viscous behavior between the materials that compose the transparent binders depending on the test condition: temperature and frequency, indicating the presence of a polymer modification in the transparent binders. Besides, the transparent binders seem to be more elastic than the conventional N50/70 binder.
- Based on the observations of the master curves and black diagram, there are no pieces of evidence that the addition of $TiO_2$ up to 10.0% significantly affects the structure or visco-elastic behavior of the transparent binders.
- The addition of $TiO_2$ seems to harm the fatigue life of the transparent binder, except for the 0.5% content, which showed a slightly improved fatigue life compared to the least performant reference binder (N50/70).
- The transparent binders present better rutting resistance than the conventional N50/70 but lower than the PMBTS. The incorporation of nano-$TiO_2$ can increase the rutting resistance for high contents (mainly 6.0% and 10.0%).
- When compared to N50/70 and PMBTS, the transparent binders showed higher indices for sulfoxides, carbonyl, polybutadiene, polystyrene, and aliphatic but lower for aromatic, branched aliphatic and long chains. The $TiO_2$ modification seems to have little effect on the indices, except for the polystyrene and aliphatic indices. The polystyrene index decreases, while the aliphatic index increases with a higher % of nano-$TiO_2$.
- Lastly, a high correlation coefficient ($R^2 = 0.99$) was witnessed for the increase of a relative index related to $TiO_2$ to the modification level and the $TiO_2$ level, confirming the assertion that nano-$TiO_2$ can be used as a marker in binder blends.

Transparent binders with $TiO_2$ give promising results, based on its conventional, rheological, and chemical performance. The best percentage of the addition of $TiO_2$, based on the results, without compromising the performance of the transparent binder, was 0.5% and 10.0% considering fatigue and permanent deformation resistance, respectively. Although the objectives of this research have been achieved, it is essential to carry out this analysis on more samples, as limited numbers were used. The next step of this research is to evaluate the light-colored and photocatalytic pavements considering the properties of color and photocatalysis.

**Author Contributions:** Conceptualization, I.R.S., E.F., and C.V., ; methodology, I.R.S., S.L.J., E.F., and C.V.; validation, J.B., T.T., S.D., and J.C.; formal analysis, I.R.S., S.L.J., A.M., and G.P.; investigation, I.R.S., E.F., C.V., T.T., S.D., and J.C.; resources, E.F., C.V., J.B., T.T., S.D., and J.C.; data curation, I.R.S., S.L.J., A.M., and G.P.; writing—original draft preparation, I.R.S., A.M., and G.P.; writing—review and editing, S.L.J., E.F., C.V., J.B., T.T., S.D., and J.C.; visualization, I.R.S, E.F, and C.V.; supervision, E.F., C.V., and J.C.; project administration,

E.F., C.V., J.C.; funding acquisition, E.F., C.V., J.B., T.T., S.D., and J.C. All authors have read and agreed to the published version of the manuscript.

**Funding:** FCT partially financed this work—Fundação para a Ciência e a Tecnologia—under the projects of the Strategic Funding UIDB/04650/2020 and UIDB/04029/2020, Nanobased concepts for Innovative and Eco-sustainable constructive material's surfaces PTDC/FIS/120412/2010. Furthermore, we would like to thank the Industrial Research Fund (IOF) of the University of Antwerp for funding the PAPPoA project (IOF/SBO/41859/2020). Lastly, the first author would like to acknowledge FCT for the PhD scholarship (SFRH/BD/137421/2018).

**Conflicts of Interest:** The authors declare no conflict of interest.

## References

[1] Chen Z, Zhang H, Zhu C, Zhao B. Rheological examination of aging in bitumen with inorganic nanoparticles and organic expanded vermiculite. Constr Build Mater 2015;101:884–91. https://doi.org/10.1016/j.conbuildmat.2015.10.153.

[2] Sengoz B, Bagayogo L, Oner J, Topal A. Investigation of rheological properties of transparent bitumen. Constr Build Mater 2017;154:1105–11. https://doi.org/10.1016/j.conbuildmat.2017.07.239.

[3] Bocci M, Grilli A, Cardone F, Virgili A. Clear Asphalt Mixture for Wearing Course in Tunnels : Experimental Application in the Province of Bolzano. SIIV - 5th Int. Congr. - Sustain. Road Infrastructures, vol. 53, Elsevier B.V.; 2012, p. 115–24. https://doi.org/10.1016/j.sbspro.2012.09.865.

[4] Guan B. Application of asphalt pavement with phase change materials to mitigate urban heat island effect. 2011 Int Symp Water Resour Environ Prot 2011:2389–92. https://doi.org/10.1109/ISWREP.2011.5893749.

[5] WHO. Ambient (outdoor) air pollution. World Heal Organ 2018. https://www.who.int/news-room/fact-sheets/detail/ambient-(outdoor)-air-quality-and-health (accessed February 4, 2020).

[6] Phua J, Weng L, Ling L, Egi M, Lim CM, Divatia JV, et al. Intensive care management of coronavirus disease 2019 (COVID-19): challenges and recommendations. Lancet Respir Med 2020;8:506–17. https://doi.org/10.1016/S2213-2600(20)30161-2.

[7] Boettler T, Newsome PN, Mondelli MU, Maticic M, Cordero E, Cornberg M, et al. Care of patients with liver disease during the COVID-19 pandemic: EASL-ESCMID position paper. JHEP Reports 2020;2:100113. https://doi.org/10.1016/j.jhepr.2020.100113.

[8] Tan W, Aboulhosn J. The cardiovascular burden of coronavirus disease 2019 (COVID-19) with a focus on congenital heart disease. Int J Cardiol 2020;309:70–7. https://doi.org/10.1016/j.ijcard.2020.03.063.

[9] Wang L, Wang Y, Ye D, Liu Q. Review of the 2019 novel coronavirus (SARS-CoV-2) based on current evidence. Int J Antimicrob Agents 2020:105948. https://doi.org/10.1016/j.ijantimicag.2020.105948.

[10] Yu H, Dai W, Qian G, Gong X, Zhou D. The NOx Degradation Performance of Nano-TiO2 Coating for Asphalt Pavement. Nanomaterials 2020;10.

[11] Rocha Segundo I, Freitas E, Landi Jr S, Costa MFM, Carneiro JO. Smart, Photocatalytic and Self-Cleaning Asphalt Mixtures: A Literature Review. Coatings 2019;9. https://doi.org/10.3390/coatings9110696.

[12] Carneiro JOO, Azevedo S, Teixeira V, Fernandes F, Freitas E, Silva H, et al. Development of photocatalytic asphalt mixtures by the deposition and volumetric incorporation of TiO2 nanoparticles. Constr Build Mater 2013;38:594–601. https://doi.org/10.1016/j.conbuildmat.2012.09.005.

[13] Rocha Segundo I, Ferreira C, Freitas EF, Carneiro JO, Fernandes F, Landi Júnior S, et al. Assessment of photocatalytic, superhydrophobic and self-cleaning properties on hot mix asphalts coated with TiO2 and/or ZnO aqueous solutions. Constr Build Mater 2018;166:36–44. https://doi.org/https://doi.org/10.1016/j.conbuildmat.2018.01.106.

[14] Hassan MM, Dylla H, Mohammad LN, Rupnow T. Evaluation of the durability of titanium dioxide photocatalyst coating for concrete pavement. Constr Build Mater 2010;24:1456–61. https://doi.org/10.1016/j.conbuildmat.2010.01.009.

[15] Yu H, Dai W, Qian G, Gong X, Zhou D, Li X, et al. The nox degradation performance of nano-tio2 coating for asphalt pavement. Nanomaterials 2020;10. https://doi.org/10.3390/nano10050897.

[16] Rocha Segundo IG da, Dias EAL, Fernandes FDP, Freitas EF de, Costa MF, Carneiro JO. Photocatalytic asphalt pavement: the physicochemical and rheological impact of TiO2nano/microparticles and ZnO microparticles onto the bitumen. Road Mater Pavement Des 2018. https://doi.org/10.1080/14680629.2018.1453371.

[17] Carnielo E, Zinzi M. Optical and thermal characterisation of cool asphalts to mitigate urban temperatures and building cooling demand. Build Environ 2013;60:56–65. https://doi.org/10.1016/j.buildenv.2012.11.004.

[18] Mirwald J, Werkovits S, Camargo I, Maschauer D, Hofko B, Grothe H. Understanding bitumen ageing by investigation of its polarity fractions. Constr Build Mater 2020;250:118809. https://doi.org/10.1016/j.conbuildmat.2020.118809.

[19] Total. Kromatis: Clear Binder for a Better Environment n.d. https://www.bitumen.total.com/bitumen-roads/kromatis (accessed October 6, 2020).

[20] Pomerantz M, Akbari H, Harvey JT. Cooler reflective pavements give benefits beyond energy savings: Durability and illumination. Proc ACEEE Summer Study Energy Effic Build 2000;8:293–304.

[21] Bocci E, Bocci M. Clear asphalt concrete for energy saving in road tunnels Clear asphalt concrete for energy saving in road tunnels. 12th Int. Soc. Asph. Pavements, 2014. https://doi.org/10.1201/b17219-219.

[22] Bocci M. Projekt INTERREG IV Innovative Beläge und Beleuchtung für Tunnel iBBT (ID 5273). Ancona: 2012.

[23] Khan MI, Sutanto MH, Sunarjono S, Room S. Effect of Crumb Rubber, Epolene (EE-2), and Date Palm Ash as Modifiers on the Performance of Binders and Mixtures: A Sustainable Approach. Sustainability 2019;11:1–13.

[24] FHA. Superpave fundamentals reference manual. 2005.

[25] RHEA. Rheology Analysis Software, version 1.2. 1, Abatech. Inc, Bloom Glen, PA 2011.

[26] Gordon G V, Shaw MT. Computer programs für rheologists. Hanser; 1994.

[27] Airey GD. Use of Black Diagrams to Identify Inconsistencies in Rheological Data. Road Mater Pavement Des 2002;3:37–41.

[28] Hintz C, Velasquez R, Johnson C, Bahia H. Modification and Validation of Linear Amplitude Sweep Test for Binder Fatigue Specification. Transp Res Rec J Transp Res Board 2011;2207:99–106. https://doi.org/10.3141/2207-13.

[29] Masad E, Somadevan N, Bahia HU, Kose S. Modeling and Experimental Measurements of Strain Distribution in Asphalt Mixes. J Transp Eng 2001;127:477–85. https://doi.org/10.1061/(ASCE)0733-947X(2001)127:6(477).

[30] Kleiziene R, Panasenkienė M, Vaitkus A. Effect of Aging on Chemical Composition and Rheological Properties of Neat and Modified Bitumen. Materials (Basel) 2019;12. https://doi.org/10.3390/ma12244066.

[31] Feng LZ, Bian H, Li X, Yu J. FTIR analysis of UV aging on bitumen and its fractions. Mater Struct 2016;49:1381–9. https://doi.org/10.1617/s11527-015-0583-9.

[32] Yut I, Zofka A. Attenuated Total Reflection (ATR) Fourier Transform Infrared (FT-IR) Spectroscopy of Oxidized Polymer-Modified Bitumens. Appl Spectrosc 2011;65:765–70. https://doi.org/10.1366/10-06217.

[33] Marsac P, Piérard N, Porot L, Van den bergh W, Grenfell J, Mouillet V, et al. Potential and limits of FTIR methods for reclaimed asphalt characterisation. Mater Struct 2014. https://doi.org/10.1617/s11527-014-0248-0.

[34] Dony A, Ziyani L, Drouadaine I, Pouget S, Faucon-Dumont S, Simard D, et al. MURE National Project: FTIR spectroscopy study to assess ageing of asphalt mixtures. Proc. E&E Congr., 2016. https://doi.org/10.14311/EE.2016.154.

[35] Zhang Z, Kang N, Zhou J, Li X, He L. Novel Synthesis of Choline-Based Amino Acid Ionic Liquids and Their Applications for Separating Asphalt from Carbonate Rocks. Nanomaterials 2019;9:5–7. https://doi.org/10.3390/nano9040504.

[36] Lamontagne J, Dumas P, Mouillet V, Kister J. Comparison by Fourier transform infrared (FTIR) spectroscopy of different ageing techniques: Application to road bitumens. Fuel 2001;80:483–8. https://doi.org/10.1016/S0016-2361(00)00121-6.

[37] Rajakumar G, Rahuman AA, Roopan SM, Khanna VG, Elango G, Kamaraj C, et al. Molecular and Biomolecular Spectroscopy Fungus-mediated biosynthesis and characterization of TiO2 nanoparticles and their activity against pathogenic bacteria. Spectrochim Acta Part A 2012;91:23–9. https://doi.org/10.1016/j.saa.2012.01.011.

[38] Jaimy KB, Ghosh S, Sankar S, Warrier KGK. An aqueous sol – gel synthesis of chromium ( III ) doped mesoporous titanium dioxide for visible light photocatalysis. Mater Res Bull 2011;46:914–21. https://doi.org/10.1016/j.materresbull.2011.02.030.

[39] Wei J, Zhao L, Peng S, Shi J, Liu Z, Wen W. Wettability of urea-doped TiO2 nanoparticles and their high electrorheological effects. J Sol-Gel Sci Technol 2008:311–5. https://doi.org/10.1007/s10971-008-1787-z.

[40] Homem NC, Beluci N de C, Amorim S, Reis R, Vieira AM, Vieira MF, et al. Applied Surface Science Surface modification of a polyethersulfone micro fi ltration membrane with graphene oxide for reactive dyes removal. Appl Surf Sci 2019;486:499–507. https://doi.org/10.1016/j.apsusc.2019.04.276.

[41] Kataware A V, Singh D. Dynamic mechanical analysis of crumb rubber modified asphalt binder containing warm mix additives. Int J Pavement Eng 2017;8436:0. https://doi.org/10.1080/10298436.2017.1380806.

[42] Airey GD. Rheological properties of styrene butadiene styrene polymer modified road bitumens. Fuel 2003;82:1709–19. https://doi.org/10.1016/S0016-2361(03)00146-7.

[43] Soenen H, Visscher J De, Vanelstraete A, Redelius P. Influence of thermal history on rheological properties of various bitumen. Rheol Acta 2006;45:729–39. https://doi.org/10.1007/s00397-005-0032-8.

[44] Hossain Z, Ghosh D. Use of the Multiple Stress Creep Recovery ( MSCR ) Test Method to Characterize Polymer - Modified Asphalt Binders. J Test Eval 2016;44. https://doi.org/10.1520/JTE20140061.

[45] Ren Z, Zhu Y, Wu Q, Zhu M, Guo F, Yu H. Enhanced Storage Stability of Different Polymer Modified Asphalt Binders through Nano-Montmorillonite Modification. Nanomaterials 2020;10:641. https://doi.org/10.3390/nano10040641.

[46] Masson JF, Pelletier L, Collins P. Rapid FTIR method for quantification of styrene-butadiene type copolymers in bitumen. J Appl Polym Sci 2001;79:1034–41. https://doi.org/10.1002/1097-4628(20010207)79:6<1034::AID-APP60>3.0.CO;2-4.

[47] Zhang H, Su M, Zhao S, Zhang Y, Zhang Z. High and low temperature properties of nano-particles/polymer modified asphalt. Constr Build Mater 2016;114:323–32. https://doi.org/10.1016/j.conbuildmat.2016.03.118.

[48] Yao H, You Z, Asce M, Li L, Lee CH, Wingard D, et al. Rheological Properties and Chemical Bonding of

Asphalt Modified with Nanosilica. J Mater Civ Eng 2013:1619–30. https://doi.org/10.1061/(ASCE)MT.1943-5533.0000690.

[49] Zhao X, Wei L, Cheng S, Huang Y, Yu Y, Julson J. Catalytic cracking of camelina oil for hydrocarbon biofuel over ZSM-5-Zn catalyst. Fuel Process Technol 2015;139:117–26. https://doi.org/10.1016/j.fuproc.2015.07.033.

[50] Cheng S, Wei L, Zhao X, Kadis E, Julson J. Conversion of Prairie Cordgrass to Hydrocarbon Biofuel over Co-Mo/HZSM-5 Using a Two-Stage Reactor System. Energy Technol 2016;4:706–13. https://doi.org/10.1002/ente.201500452.

[51] Zajíčková L, Buršíková V, Kučerová Z, Franclová J, Sťahel P, Peřina V, et al. Organosilicon thin films deposited by plasma enhanced CVD: Thermal changes of chemical structure and mechanical properties. J Phys Chem Solids 2007;68:1255–9. https://doi.org/10.1016/j.jpcs.2007.02.044.

[52] Urda A, Popescu I, Marcu IC, Carja G, Apostolescu N, Sandulescu I. Methane and propane total oxidation on catalysts from FeLDH precursors. Rev Chim 2010;61:267–71.

[53] Yaseen M, Shah Z, Veses RC, Dias SLP, Lima EC, S dos Reis G, et al. Photocatalytic Studies of TiO2/SiO2 Nanocomposite Xerogels. J Anal Bioanal Tech 2017;08:8–11. https://doi.org/10.4172/2155-9872.1000348.

[54] Jiang Y, Gu X, Zhou Z, Ni F, Dong Q. Laboratory Observation and Evaluation of Asphalt Blends of Reclaimed Asphalt Pavement Binder with Virgin Binder using SEM / EDS. Transp Res Rec 2018:1–10. https://doi.org/10.1177/0361198118782023.

[55] Rinaldini E, Schuetz P, Partl MN, Tebaldi G, Poulikakos LD. Investigating the Blending of Reclaimed Asphalt with Virgin Materials using Rheology, Electron Microscopy and Computer Tomography. Compos PART B 2014. https://doi.org/10.1016/j.compositesb.2014.07.025.

[56] Sun SS, Wang YM, Zhang AQ. Study on Anti-Ultraviolet Radiation Aging Property of $TiO_2$ Modified Asphalt. Adv Mater Res 2011;306–307:951–5. https://doi.org/10.4028/www.scientific.net/AMR.306-307.951.

[57] Zhang W, Shi J, Jia Z. The UV anti-aging performance of TPS modified bitumen. Pet Sci Technol 2018;36:1–6. https://doi.org/10.1080/10916466.20138.1465962.